J. Fluid Mech. (1964), *vol.* 20, *part* 3, *pp.* 513–527
Printed in Great Britain

Experiments on the lift and drag of spheres suspended in a Poiseuille flow

By R. EICHHORN AND S. SMALL*

Department of Aerospace and Mechanical Sciences,
Princeton University, Princeton, N.J.

(Received 3 February 1964)

An experimental investigation of the fluid dynamic forces on spheres suspended in a Poiseuille flow was performed. Small spheres of polystyrene, nylon, and Lucite, having diameters ranging from 0·061 in. to 0·126 in. were suspended in Poiseuille flows in a 0·419 in. diameter tube. Variations in particle size and density, the fluid properties, and the angle of inclination of the tube, resulted in a sphere Reynolds number (based on particle diameter and approach velocity) ranging from 80 to 250. The results are presented as curves which include the coefficients of lift and drag, and the dimensionless rotation speed plotted versus Reynolds number and a dimensionless shear parameter.

Introduction

We are concerned, in this paper, with the forces on spheres in a Poiseuille flow. The net force on such a sphere can be resolved into components along and normal to the direction of the approaching flow. We choose to term the former a drag force (F_D) and the latter a lift force (F_L). The lift force, not usually encountered in discussions of the flow about spheres, is a consequence of the velocity gradient and results from an asymmetric surface pressure distribution.

In the course of many years, much attention has been given to the theory of viscous flow about a sphere both in an unbounded medium and in media bounded by cylinder walls. Because of the complexity of the general Navier–Stokes equation, most of the theoretical approaches have assumed a very low Reynolds number. In this régime the Navier–Stokes equation can be simplified to a linear, fourth-order, partial-differential equation. The first boundary condition imposed was that of a uniform unbounded flow (Lamb 1932) and then, later, flows within an infinitely long cylindrical tube were considered (Ladenburg 1907; Faxen 1922; Lee 1947; Haberman & Sayre 1958). Finally, Poiseuille flows about a sphere in a cylinder have been treated (Haberman & Sayre 1958; Happel & Byrne 1954; Wakiya 1953; Brenner & Happel 1958).

Analysis of the flow about spheres at very low Reynolds numbers allows the calculation of drag but not of lift, since the inertial effects, from which the lift must result, are neglected. The general procedure has been to present the results of bounded flows as a correction factor to the Stokes drag on a sphere in a uniform, unbounded flow. Attempts have also been made to calculate the drag when the

* Present address: Bureau of the Budget, Washington, D.C.

inertia terms have been partially accounted for; e.g. on the basis of the Oseen equation of flow. More recently, Rubinow & Keller (1961) have estimated the lift on a rotating sphere at small Reynolds numbers in Poiseuille flow.

Experimentally, the curve of drag coefficient versus Reynolds number for spheres in an unbounded fluid has been the object of continued attention for the Reynolds number range $10^{-1} < Re < 10^{6}$ (Perry 1950). For spheres bounded by cylinder walls, experiments have been chiefly of the sedimenting sphere variety (McNown, Lee, McPherson & Engez 1948; Fidleris & Whitmore 1961). Recently, Fayon & Happel (1960) performed experiments in which a sphere was held fixed in a Poiseuillian flow at various distances from the axis. The flow was vertically upwards and the drag was measured. Their results yielded a semi-empirical equation for $Re < 40$.

To the authors' knowledge, no direct experimental data for the lift forces on spheres in a velocity gradient at low Reynolds numbers have been reported heretofore, although such effects have been studied indirectly, as, for example, in the work of Young (1960) and Segré & Silverberg (1961, 1962*a*, *b*). The latter authors note a reversal in sign of the lift force such that spheres situated at a radius less than a certain value are forced outward while those beyond that radius are forced inward. Due to the high Reynolds numbers in the present study, a comparison of the results with those of Segré & Silverberg is probably not meaningful.

Considerable work has been done on the problem of an inviscid flow with a velocity gradient about spheres and cylinders (Tsien 1943; Lighthill 1957; Zierep 1955; Hall 1956). Much of this work bears on the pitot-probe displacement problem.

In this paper, experimental measurements are presented of the lift, drag and speed of rotation of spheres in velocity gradients in a Reynolds number range beyond the Stokes régime. In contrast to the work by Fayon & Happel (where the particle was held fixed in the flow), this experiment suspended particles freely, using the fluid dynamic forces to hold a particle at rest.

Specifically, small spheres were suspended in a 0·419 in. diameter tube containing a laminar upward flow of water. The tube was inclined to the vertical and the flow rate was adjusted to bring the sphere to rest at a fixed distance from the tube wall. In this position, the apparent weight of the sphere is balanced by the lift force toward the tube axis due to the velocity gradient (i.e. the asymmetrical pressure recovery) and the drag force due to the longitudinal flow. Thus, if the particle and fluid densities are known, as well as the tube inclination and radial position of the particle, the lift and drag forces can be determined.

Description of apparatus

The experiments were performed with the apparatus shown in figures 1 and 2. The principal element, a glass tube of internal diameter 0·419 in. is shown in figure 1 and a line diagram of the flow system in figure 2.

The glass tube in which the sphere suspension measurements were performed was 40 in. in length and was provided with entrance and exit sections 6 in. long and 2 in. in diameter. The inlet (lower) section was carefully fused to the main

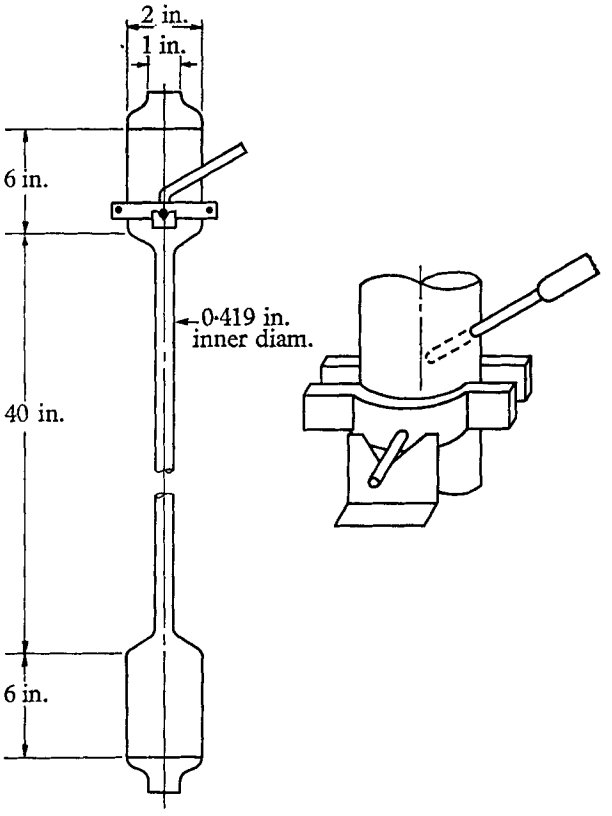

FIGURE 1. Tube and mounting arrangement in a vee-notch.

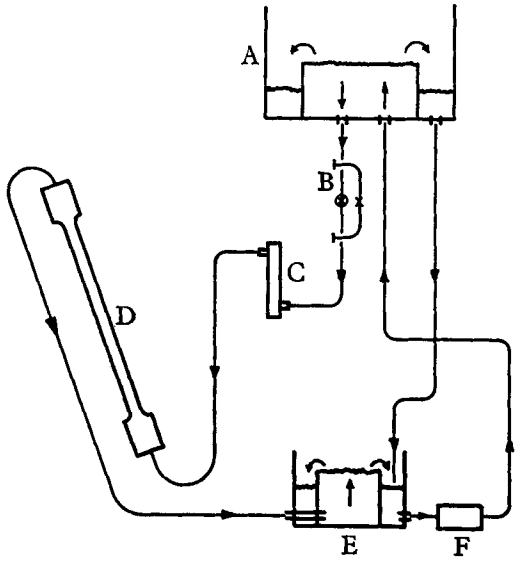

FIGURE 2. Line diagram of flow system: A, upper constant head tank; B, gate and needle valves in parallel; C, flowrator; D, tube; E, lower constant head tank; F, gear pump.

tube. A rounded entrance was provided. The exit (upper) section was supported by pins resting in a vee-notch. Rotation in a vertical plane was thus assured. The vertical alignment was continually checked with a transit. Spheres to be studied were introduced through a $\frac{1}{4}$ in. diameter tube fused into the exit section.

In order to avoid pressure fluctuations, constant-head tanks were installed to serve as the driving potential for the flow; a gear pump being used to return the flow to the upper tank. Coarse and fine adjustment of the mass flow was obtained by placing in parallel a 1 in. gate valve and a $\frac{1}{4}$ in. needle valve. The mass flow was measured by a rotameter (Fisher–Porter 'Flowrator') which was first carefully calibrated.

The radial position of the particle and the angle of inclination of the tube were determined from photographs of a section of the tube. The tube angle was obtained by reference to a vertical nylon thread photographed along with the particle. The camera was a Polaroid Land type 110 A used with Type 3000 film. The speed of rotation was determined visually by counting a number of revolutions against a stop-watch.

In the design of the apparatus, consideration was given to tube size, flow rate and sphere diameter and weight. Operating characteristics were calculated approximately to insure that the tube Reynolds number would be small enough to avoid either incipient transition to turbulence or unduly long entrance lengths. A conservative estimate for the entrance length was deduced from the measurements of Nikuradse (Schlichting 1960), according to whom the entrance length L_e in tube diameters can be estimated by the formula $L_e/D = 0{\cdot}06\,Re_D$, where the Reynolds number is based on the mean flow velocity. In all the measurements reported here, this criterion was satisfied.

Experimental procedure

The experimental procedure can be conveniently separated into three phases: (I) events prior to the test runs, (II) the test runs, and (III) the events succeeding the test runs.

I. Prior to the test runs the properties of the particle were determined. With the use of a pyncnometer bottle and analytical balance, the specific gravity and diameter were measured. These results are shown in table 1. No special attempts to determine sphericity were made, but the spheres employed were selected after observation under magnification.

II. Tests were conducted with four spheres composed of three different plastic materials. The tests were performed in the following way: beginning with the tube vertical, a particular particle was selected and introduced into the stream. Care was taken that no air was allowed to leak into the stream. Adjustment of the flow, via the control valves, brought the particle to rest. A photograph was taken and the flowrator and temperature readings were recorded. At this time, the rotation speed was determined. The mass flow was then increased sufficiently to suspend the sphere in the upper 2 in. diameter section while the tube was re-set at some desired angle of inclination. After checking the tube alignment, the mass flow was reduced and adjusted, again bringing the particle to rest in the test section. The procedure was repeated until the test series was complete.

III. The final phase of the experiment consisted of a study of the photographs; i.e. the determination of the angle of inclination and the radial displacement of the particle. Both were determined directly with the use of a magnifying glass and scale. The angle of inclination was determined by geometrical considerations as described in figure 3. The measured radial position was corrected for refraction effects using handbook values for the refractive indices of glass and water.

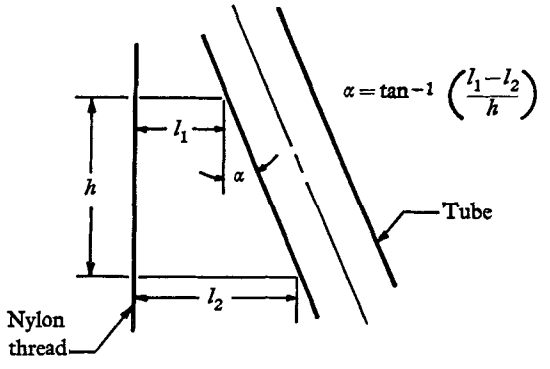

FIGURE 3. Illustration of tube inclination measurement.

Sphere no.	Diameter (in.)	Specific gravity	Symbol used on graphs
1	0·126	1·066	○
2	0·094	1·258	▽
3	0·062	1·144	△
4	0·061	1·426	◇

TABLE 1. Properties of the spheres.

Following the experimental procedure as outlined, the basic data was obtained. These results are given in the Appendix and shown plotted in figures 4, and 6 to 11 inclusive.

Discussion of results

Drag

The drag of a sphere suspended in an inclined tube is merely the longitudinal component of the force required to keep the sphere motionless. Thus

$$F_D = W \cos\alpha,$$

where F_D is the drag, W is the apparent weight of the sphere, and α is the angle of inclination of the tube. The drag coefficient is then

$$C_D = F_D/(\tfrac{1}{2}\rho u^2)\pi a^2, \tag{1}$$

where u is the approach velocity toward the sphere centre. For a parabolic velocity-profile $u = u_0(1-\beta^2)$, u_0 being the velocity at the tube centre-line, and β the non-dimensional radial displacement b/R.

The drag coefficient versus the particle Reynolds number, Re_p, based on approach velocity and sphere diameter, is shown in figure 4. For reference the

accepted curve for spheres in an unbounded medium (Perry 1950, p. 1018) is also shown. For each run, data are shown for an axially located particle and for particles of increasing displacement (i.e. increased tube inclination) up to the point where the sphere touches the wall. For greater tube inclinations, the sphere continually bumps against the wall.

Since we are considering a case in which the sphere is at rest in a laboratory frame of reference, the drag coefficient can depend only on the Reynolds number, Re_p, a dimensionless displacement, β, and the sphere to tube diameter ratio, d/D,

$$C_D = C_D(Re_p, \beta, d/D). \tag{2}$$

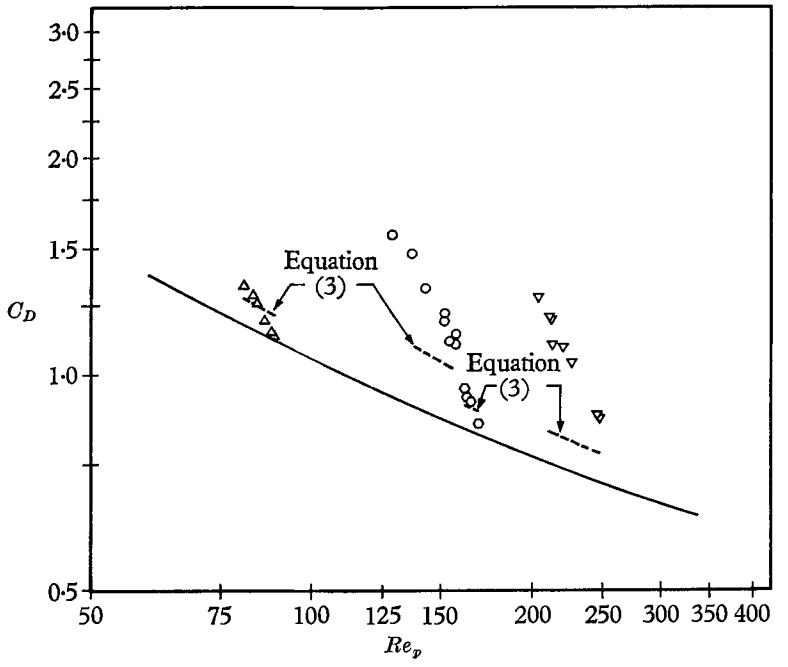

FIGURE 4. Drag coefficient *vs* particle Reynolds number: ○, sphere no. 1; ▽, sphere no. 2; △, sphere no. 3; ⬡, sphere no. 4; ——, sphere in unbounded medium (Perry 1950); – – –, equation (3). Not all data points are shown.

To help interpret this relationship and thus the data in figure 4, the schematic representation of figure 5 has been prepared. In figure 5 (*a*), the relationship of equation (2) to d/D is shown parametrically so that C_D (Re_p, β) is represented as a surface. A curve of C_D *vs* Re such as is shown in figure 4 results not only from the variation of C_D with Re but also, and in this case primarily, with β. This fact is illustrated in figure 5 (*b*), where the operating curve (line 1) of the apparatus as traced out on the C_D (Re_p, β) surface and projected (line 2) onto the (C_D, Re_p)-plane is shown.

Consider the data represented by one value of d/D, say, for example, those given by ▽ (runs 45 to 52) in figure 4. The calculated maximum error in C_D for runs 45 and 48 was $\pm 10\%$ and $\pm 17\%$, respectively. In both cases, the maximum error in the Reynolds number was less than $\pm 5\%$. These errors result from various uncertainties in the measurements, primarily sphere radius, sphere

density, tube radius, flow rate and sphere position. The first three listed sources of error, although perhaps random in origin, are systematic when one compares measurements made with a given sphere in a given tube. Thus, although the

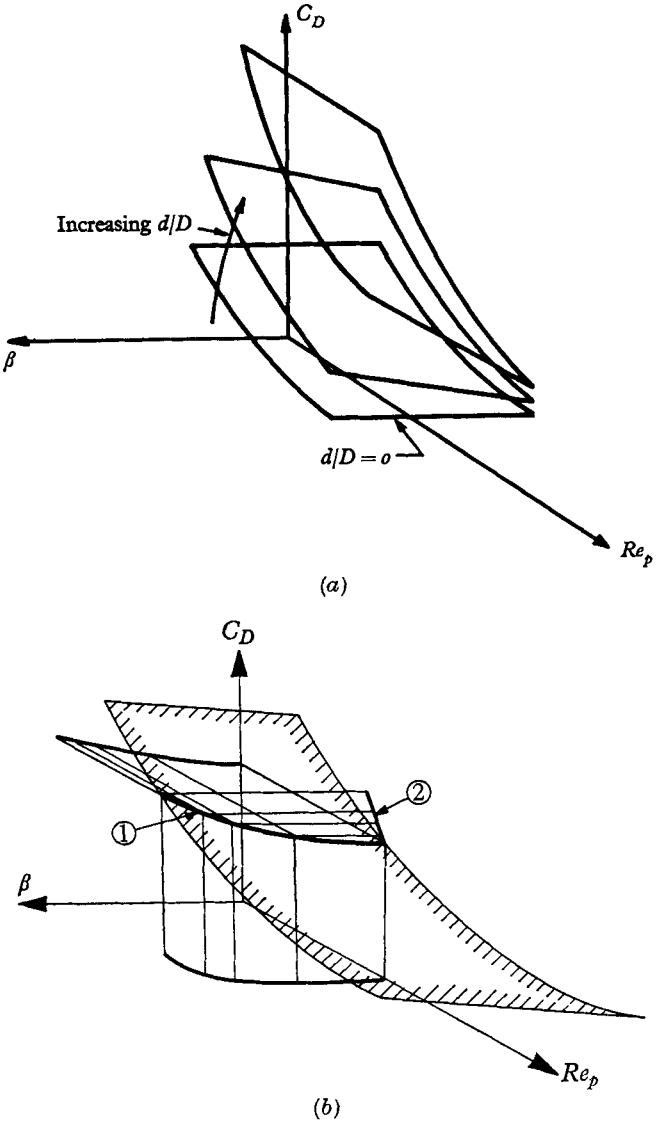

FIGURE 5. Schematic diagram of the relation $C_D = C_D(Re_p, \beta, d/D)$. ① Operating curve determined by system characteristics; ② projection of ① on (C_D, Re_p)-plane.

absolute value of C_D for run 48 cannot be certified to better than $\pm 17\,\%$, a large portion of this error becomes systematic when one compares C_D for run 48 with that for run 45. In considering the difference in drag coefficient even within a single set of data, one must sum the remaining random errors. For the above case this gives a maximum error of $\pm 10\,\%$, which, although still quite high, is tolerable in the light of the large observed changes in drag coefficient.

The only previously published expression known to the authors for predicting the changes in drag coefficient is the semi-empirical formula of Fayon & Happel (1960), which can be written as

$$C_D = C_A + C_S \left[\frac{2{\cdot}105(d/D) - 2{\cdot}087(d/D)^3 - \frac{2}{3}(1-\beta^2)^{-1}(d/D)^2}{1 - 2{\cdot}105(d/D) + 2{\cdot}087(d/D)^3} \right], \tag{3}$$

where C_A is the drag coefficient for an unbounded sphere, and C_S is the Stokes drag coefficient. The predictions resulting from the application of this formula are shown in figure 4. Fayon & Happel of course did not intend equation (3) to be used at Reynolds numbers as high as those encountered here, nor indeed for the case of a freely rotating sphere. However, equation (3) fails to predict the trend of the data because the coefficient of the term accounting for effects of β and d/D is the Stokes drag coefficient which decreases with Reynolds number much faster than does C_A. In fact, the variation of C_D with Re_p as calculated from (3) and shown in figure 4 is due almost entirely to changes in C_A and hardly at all to changes in β.

In view of the present state of our theoretical knowledge, it seems best to attempt a direct correlation of the data. Returning to equation (2), we will assume that the Reynolds number variation is of the power-law variety, so that (2) can be written

$$C_D = Re_p^n f(\beta, d/D).$$

Then the drag coefficient where $\beta = 0$ is given by

$$C_{D0} = Re_{p0}^n f(0, d/D).$$

From these two expressions, we can form the ratio

$$\frac{C_D}{C_{D0}} \left(\frac{Re_p}{Re_{p0}} \right)^{-n} = \frac{f(\beta, d/D)}{f(0, d/D)}. \tag{4}$$

The left-hand side of (4) is shown plotted against $(1-\beta^2)^{-1}$ in figure 6. In each case, the value of n used is that corresponding to the variation of C_A in the centre of the appropriate Reynolds number range. From figure 6, it appears that the effect of variations with β are fairly well delineated and that the two lines shown have different slopes resulting from changes in d/D. The data for the two $\frac{1}{16}$ in. spheres (nos. 3 and 4) fall on the same line even though the Reynolds numbers are different by a factor of two. A possible blemish on this correlation is indicated by the fact that no significant difference exists between the data for the $\frac{3}{32}$ and $\frac{1}{8}$ in. spheres (nos. 1 and 2).

From figure 6 and equation (4), we can write the final result as

$$C_D = Re_p^n f(0, d/D) \left[1 + F(d/D) \left(\frac{\beta^2}{(1-\beta^2)} \right) \right], \tag{5}$$

where $F(d/D)$ is the slope of a line of constant d/D in figure 6.

Unfortunately, the data are not sufficiently extensive or accurate to make definitive statements about the form of $Re^n f(0, d/D)$.

The Fayon & Happel expression (3) predicts the drag coefficient for $\beta = 0$ within the experimental uncertainty, and can be combined with (5), replacing the unknown function $Re_p^n f(0, d/D)$.

Rotation

In the experiment described above, spherical particles were suspended, at increasing displacement, in a parabolic velocity field. If the particle is assumed to be a small fluid element and the flow is assumed to be viscous, then the rigid body rotation of such an element has the simple theoretical value of $\frac{1}{2}(du/dy)$.

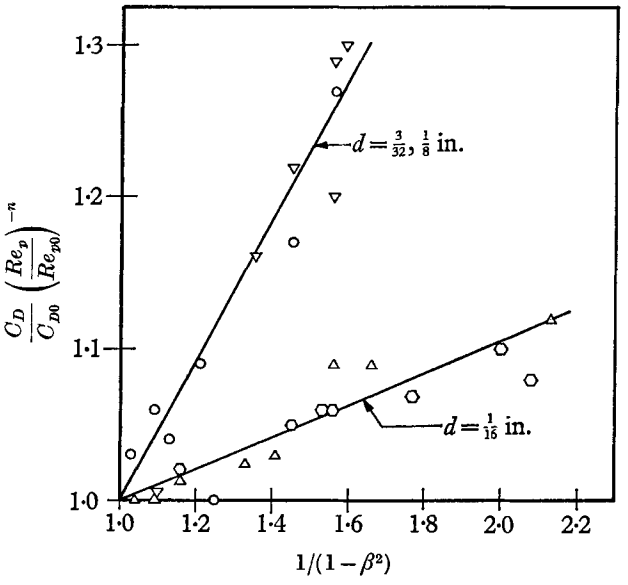

FIGURE 6. Drag-coefficient correlation.

Consider figure 7 which shows a plot of the non-dimensional experimental angular velocity versus the non-dimensional shear. From dimensional analysis, one must anticipate a functional relationship of the form

$$\frac{\omega_e}{\frac{1}{2}du/dy} = \frac{\omega_e R}{\beta u_0} = f\left[Re_p, \frac{d}{D}, \frac{d}{u}\left(\frac{du}{dy}\right)\right], \dagger \tag{6}$$

where ω_e is the angular velocity of rotation and R is the tube radius. However, an inspection of the curves reveals that the spread between runs is a Reynolds number effect since the two runs at nearly the same Reynolds number, but different diameter ratios, are brought together when plotted this way. Based on this limited data, we would conclude that

$$\frac{\omega_e R}{\beta u_0} = f\left[Re_p, \frac{d}{u}\left(\frac{du}{dy}\right)\right].$$

Next consider figure 8 in which we attempt to eliminate the Reynolds number effect by plotting $(\omega_e R/\beta u_0)Re_p$ versus the dimensionless shear. Although some

† As with the drag coefficient, the rotation coefficient must be a function of the variables Re_p, d/D and β. However, since the rotation is intimately related to the presence of shear, we adopt instead the entirely equivalent set of parameters Re_p, d/D and $(d/u)du/dy$, the latter being a non-dimensional shear parameter. The hope here is that the results will thus be more general.

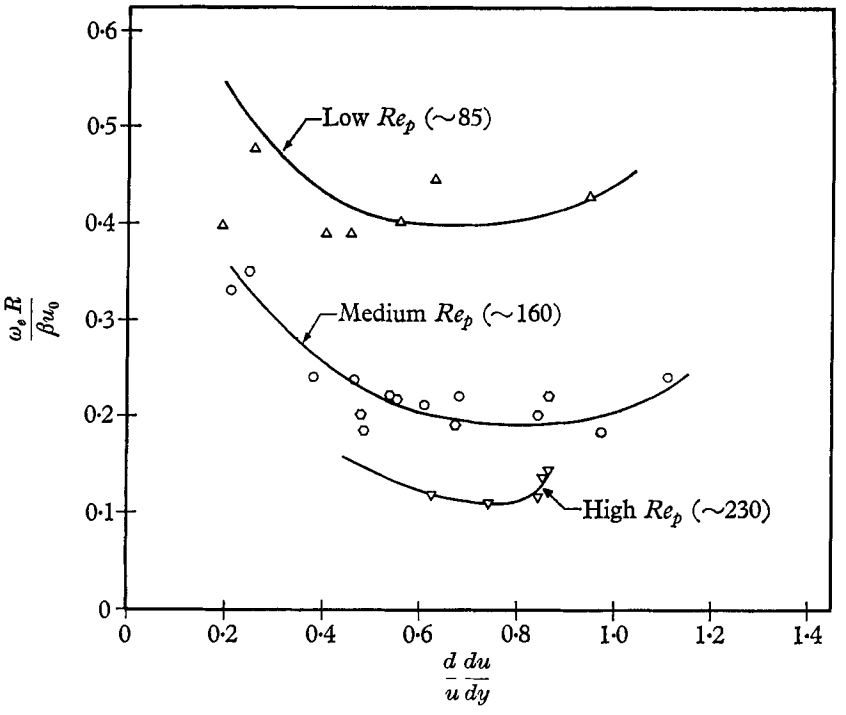

FIGURE 7. Experimental rotation speed *vs* shear parameter.

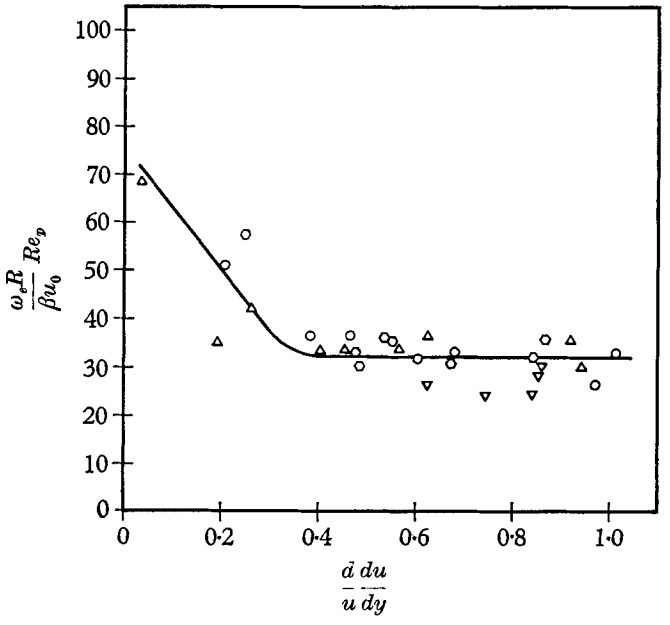

FIGURE 8. Correlation of rotation speeds.

systematical differences between the runs still exist, it seems reasonable to postulate an equation of the form

$$\frac{\omega_e R}{\beta u_0} = (Re_p)^{-1} f\left[\frac{d}{u}\left(\frac{du}{dy}\right)\right].$$

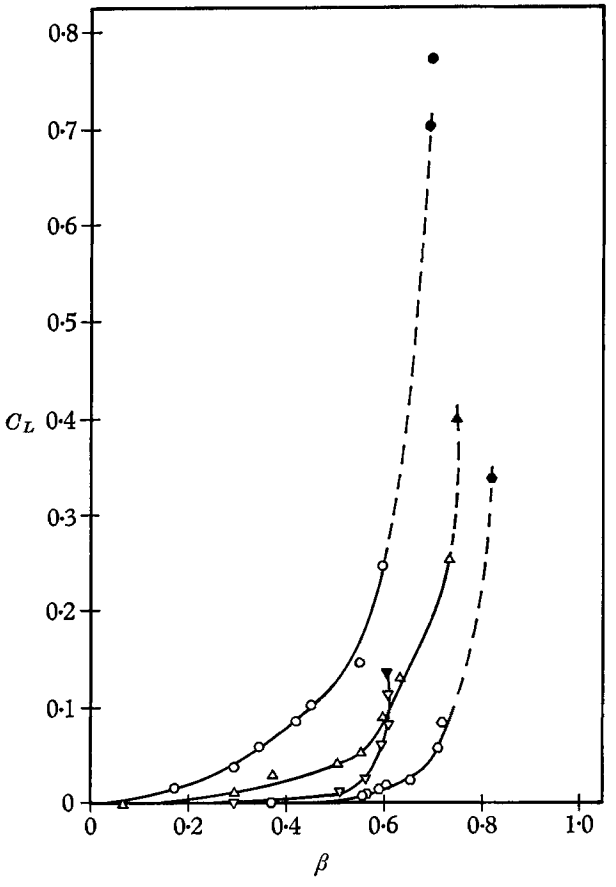

FIGURE 9. Lift coefficient *vs* displacement from centre-line.

For $0{\cdot}4 < (d/u)\,(du/dy) < 1{\cdot}0$, we have as a further approximation

$$\omega_e R/\beta u_0 \simeq 32/Re_p. \tag{7}$$

We note that the angular velocity decreases with increasing Reynolds number, which we would expect. It must be pointed out, however, that the above approximation has limited applicability since it predicts that the angular velocity would approach very large values as the Reynolds number becomes small.

Lift

The lift force acting on a sphere in an inclined tube is the radial component of the force required to keep the sphere motionless. Thus,

$$F_L = W \sin\alpha,$$

where F_L is the lift and the other variables remain as described earlier. In a similar fashion the lift coefficient is then

$$C_L = F_L/\tfrac{1}{2}\rho u^2 \pi a^2.$$

A dimensional analysis gives the relationship (see footnote on p. 9)

$$C_L = C_L(Re_p, d/D, (d/u)\,(du/dy)).$$

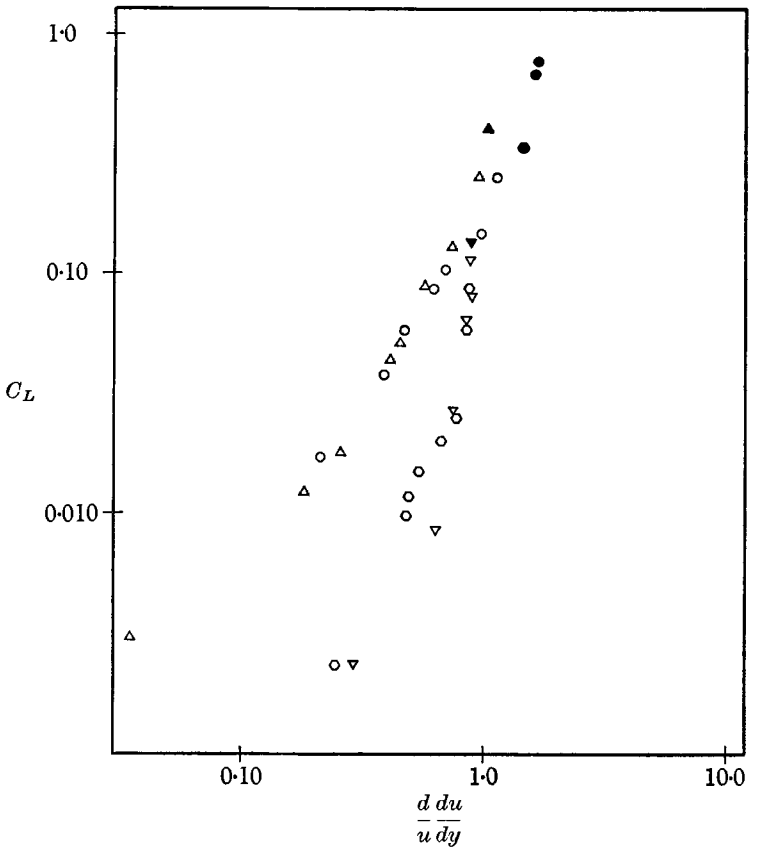

FIGURE 10. Lift coefficient *vs* shear parameter.

The following paragraphs will attempt to shed some light on the complicated relationships described by this formula. However, since it will be seen that the experimental data available contain a relatively high degree of scatter, we shall mainly attempt to obtain a relationship which is qualitative in nature, and in the process use arguments which tend to be somewhat intuitive.

Figure 9 shows the coefficient of lift plotted against the dimensionless displacement β. In this figure the lift coefficients obtained when the particle bumped against the wall are plotted as solid symbols. The data plotted in this way fail to reveal any systematic trend either with diameter ratio or Reynolds number. This fact justifies, to an extent, our attention to the shear parameter $(d/u)\,(du/dy)$. An attempt at correlation on this basis is shown in figure 10 where C_L is plotted

vs the shear parameter on log co-ordinates. Here again, no systematic trend with either diameter ratio or particle Reynolds number is revealed. However, we now note that the dependency of C_L on $(d/u)\,(du/dy)$ is nearly as the square of the latter. This clearly identifies the effect as inertial, since the rotation speed of

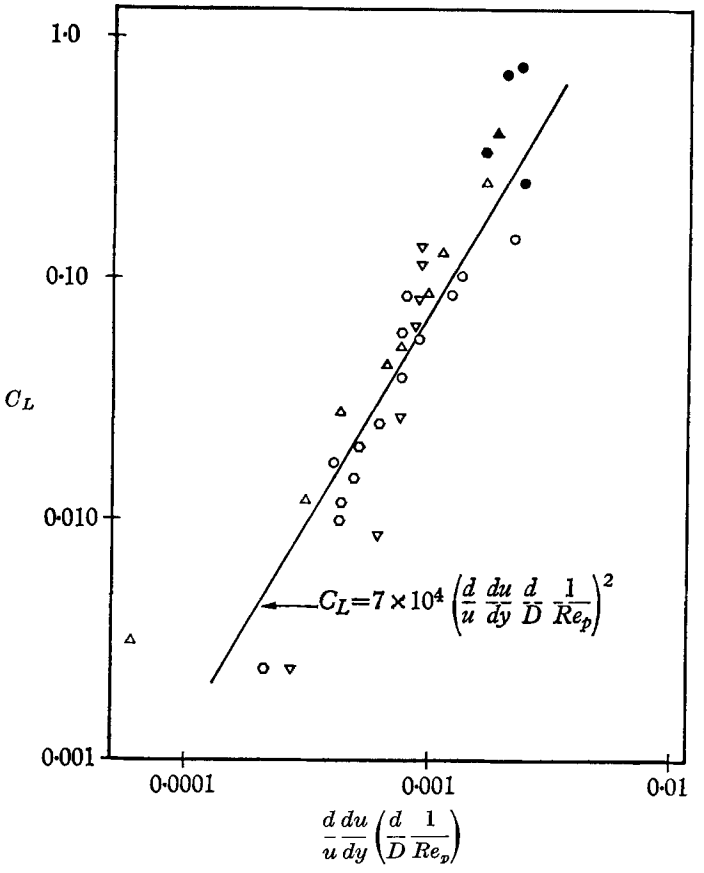

FIGURE 11. Correlation of lift coefficient.

the particle is also related to the shear parameter (cf. figure 8 and equation (7)). In fact, a plot of C_L *vs* $\omega_e d/u$ reveals an even closer square dependency than that shown in figure 9. This being a relationship between two dependent variables, however, it is not presented here.

Closer examination of figure 10 shows that the effects of Reynolds number and diameter ratio work in opposite directions, i.e. C_L decreases with increasing Reynolds number and increases with decreasing diameter ratio. The plot in figure 11 was prepared in an attempt to take these facts into account. The data appear to be brought together somewhat better than before, although it must be admitted that this may be fortuitous in view of the small number of cases represented. The line shown in the diagram was drawn by eye and is represented by the equation

$$C_L = 7 \times 10^4 \left[\left(\frac{d}{u}\frac{du}{dy}\right)\frac{d}{D}\frac{1}{Re_p}\right]^2.$$

Only a tentative recommendation can be made for the formula.

A theoretical prediction by Rubinow & Keller (1961) shows $C_L \propto (d/u)\, du/dy$ in the Stokes–Oseen range. From the data presented here, it appears that the Rubinow & Keller prediction does not hold beyond the Stokes–Oseen régime.

Conclusions

A technique for determining the forces acting on spheres suspended in a laminar tube flow has been devised and tested. The results, although not extensive, provide new information about the drag on spheres in such flows and the first direct measurements known to the authors of lift forces resulting from a velocity gradient in the flow.

The chief drawbacks of the technique are the extremely accurate measurements required (not entirely achieved in this study), and the fact that important variables (such as rotation speed and radial position) are related by the operating characteristics of the apparatus and thus cannot be varied independently by the experimenter.

This work was sponsored by Project SQUID, which is supported by the Office of Naval Research, Department of the Navy, under Contract No. 3623 (00), NR-098-038. Reproduction in full or in part is permitted for any use of the United States Government.

REFERENCES

BRENNER, H. & HAPPEL, J. 1958 *J. Fluid Mech.* **4**, 195.

FAXEN, H. 1922 *Arkiv f. Math., Astro. och Fysik*, **17**, no. 27.

FAYON, A. M. & HAPPEL, J. 1960 *A.I.Ch.E.J.* **6**, 55.

FIDLERIS, V. & WHITMORE, R. L. 1961 *Brit. J. Appl. Phys.* **12**, 490.

HABERMAN, W. L. & SAYRE, R. M. 1958 *David Taylor Model Basin, Rep.* no. 1143.

HALL, I. M. 1956 *J. Fluid Mech.* **1**, 142.

HAPPEL, J. & BYRNE, B. J. 1954 *Indust. Engng Chem.* **46**, 1181.

LADENBURG, R. 1907 *Ann. Phys.* (Ser. 4), **23**, 447.

LAMB, H. 1932 *Hydrodynamics*, 6th ed. New York: Dover.

LEE, H. M. 1947 A Modification of Stokes' Law to Account for Boundary Influence, M.S. Thesis, State University of Iowa.

LIGHTHILL, M. J. 1957 *J. Fluid Mech.* **2**, 493.

MCNOWN, J. S., LEE, H. M., MCPHERSON, M. B. & ENGEZ, S. M. 1948 *Proc. 7th Inter. Cong. Appl. Mech. (London)*, **2**, 17.

OSEEN, C. W. 1910 *Arkiv f. Math., Astro. och Fysik*, **6**, no. 29.

PERRY, J. H. 1950 *Chemical Engineering Handbook*, 3rd Ed. New York: McGraw-Hill.

RUBINOW, S. I. & KELLER, J. B. 1961 *J. Fluid Mech.* **11**, 447.

SCHLICHTING, H. 1960 *Boundary Layer Theory*, 4th Ed., p. 257. New York: McGraw-Hill.

SEGRÉ, G. & SILVERBERG, A. 1961 *Nature, Lond.*, **189**, 209.

SEGRÉ, G. & SILVERBERG, A. 1962*a* *J. Fluid Mech.* **14**, 115.

SEGRÉ, G. & SILVERBERG, A. 1962*b* *J. Fluid Mech.* **14**, 136.

TSIEN, H. S. 1943 *Quart. Appl. Math.* **1**, 130.

WAKIYA, S. 1953 *J. Phys. Soc. Japan*, **8**, 254.

YOUNG, D. F. 1960 *A.S.M.E. Paper* 60-HYD-12.

ZIEREP, J. 1955 *Z. f. Flugwiss.* **3**, 22.

Appendix

Run no.	u (ft./sec)	Re_p	β	α (deg)	ω_e (sec^{-1})	C_D	C_L
			Sphere no. 1				
35	0·164	157	0·00	0·00	0·00	1·10	0·00
36	0·162	155	0·17	0·78	0·53	1·13	0·017
37	0·158	151	0·29	1·87	0·69	1·19	0·039
38	0·162	156	0·34	2·95	0·84	1·14	0·058
39	0·156	150	0·42	4·03	0·96	1·21	0·086
40	0·159	153	0·45	5·27	1·10	1·11	0·103
41	0·149	144	0·56	6·30	1·27	1·33	0·147
42	0·141	137	0·60	7·64	1·78	1·48	0·250
43*	0·115	233	0·69	18·4	4·19	2·12	0·704
44*	0·121	211	0·70	22·5	4·84	1·86	0·773
			Sphere no. 2				
45	0·315	247	0·00	0·00	0·00	0·87	0·00
46	0·314	246	0·30	0·015	—	0·88	0·002
47	0·289	226	0·51	0·47	1·34	1·04	0·009
48	0·281	220	0·56	1·40	1·48	1·10	0·027
49	0·270	212	0·60	3·27	1·68	1·10	0·063
50	0·269	211	0·60	3·88	1·96	1·19	0·081
51	0·268	210	0·61	5·43	2·13	1·20	0·114
52*	0·270	212	0·61	6·52	2·52	1·18	0·135
			Sphere no. 3				
53	0·330	169	0·00	0·00	0·00	0·86	0·00
54	0·322	165	0·37	0·015	7·78	0·89	0·002
55	0·320	164	0·56	0·62	12·4	0·91	0·010
56	0·320	165	0·56	0·75	12·7	0·91	0·012
57	0·318	164	0·59	0·94	13·5	0·92	0·015
58	0·316	162	0·60	1·25	14·5	0·93	0·020
59	0·314	162	0·66	1·55	17·3	0·94	0·026
60	0·312	162	0·71	3·58	22·0	0·96	0·060
61	0·311	161	0·72	5·01	26·4	0·95	0·084
62*	0·241	125	0·82	12·2	33·9	1·56	0·338
			Sphere no. 4				
63	0·168	89	0·00	0·00	0·00	1·13	0·00
64	0·168	89	0·06	0·015	0·68	1·13	0·003
65	0·167	99	0·29	0·62	3·22	1·14	0·012
66	0·167	88	0·37	1·57	4·15	1·15	0·028
67	0·165	87	0·50	2·18	6·36	1·18	0·044
68	0·164	86	0·54	2·97	7·16	1·19	0·052
69	0·160	84	0·60	4·00	8·66	1·26	0·088
70	0·157	83	0·63	5·72	9·49	1·29	0·129
71	0·154	81	0·73	10·8	13·9	1·33	0·253
72*	0·151	80	0·75	16·6	14·6	1·34	0·401

* Cases for which the sphere bumped against the tube wall.